

# **An electrodeposited Ni-P-WS<sub>2</sub> coating with combined super-hydrophobicity and self-lubricating properties**

Y. He,<sup>1,2</sup> S.C. Wang,<sup>1</sup> P.A.S. Reed,<sup>3</sup> W.T. Sun,<sup>4</sup> F.C. Walsh<sup>1</sup>

<sup>1</sup> National Centre for Advanced Tribology at Southampton (nCATS), University of Southampton, SO17 1BJ, UK.

<sup>2</sup> Centre for Composite Materials and Structures, Harbin Institute of Technology, Harbin 150080, PR China

<sup>3</sup> Engineering Materials and Surface Engineering, University of Southampton, SO17 1BJ, UK.

<sup>4</sup> School of Material Science and Engineering, Harbin Institute of Technology, Harbin 150001, PR China

## **Abstract**

Self-lubrication and super-hydrophobicity are sought-after qualities in industrial surface finishing but such properties are rarely combined in a single coating. The present studies have produced a low-friction, superhydrophobic Ni-P-WS<sub>2</sub> coating by a versatile one-pot, single-step electrodeposition. By adjusting the particle and surfactant concentrations, a hierarchical surface, consisting of micron-sized protrusion arrays and submicron-sized bumps on the top and exhibiting a high water contact angle of 157 deg was achieved. Furthermore, mechanical and friction properties are characterized, revealing that sufficient WS<sub>2</sub> embedded in the Ni-P coatings enables a reduced friction coefficient of 0.17 by the formation of a self-lubricating tribofilm.

**Keywords:** dual-scale; electrodeposition; Ni-P; self-lubrication; super-hydrophobicity, WS<sub>2</sub>,

## 1 Introduction

Super-hydrophobic surfaces, with a water contact angle, WCA >150 deg, have gained more and more attention for their practical applications in the fields of self-cleaning, anti-corrosion, anti-fouling, frost prevention and energy saving. Super-hydrophobicity can be achieved by modifying a surface with low surface free energy organic chemicals or/and creating a rough but hierarchical surface morphology [1]. However, these organic chemicals are easily removed and the super-hydrophobicity cannot be sustained. In addition, the most common fluorine-containing chemicals, such as fluoroalkyl silanes, fluoropolymers and fluorosurfactants, are persistent and environmentally hazardous [2, 3, 4]. Several techniques, including lithographically fabricated surfaces, thermal spraying and sol-gel, have been used to fabricate inorganic super-hydrophobic surfaces. However, these approaches require either complex processes or special equipment. Electrodeposition is a versatile technique which avoids the need for expensive equipment or a specialised reaction environment [2]. Moreover, it is traditionally suited to industrial scale-up. A large variety of super-hydrophobic films including Ni [3,4], Co [5], Cu [6], Ce [7] and metal composite films [8,9] have been successfully prepared by modifying the deposition parameters, adding cationic surfactants and embedding of particles into a coating matrix.

The introduction of nanoparticles into a metal electrodeposit can alter surface roughness, resulting in a variation in wetting properties. Nanoparticles with low surface energy, such as laminar structures of MoS<sub>2</sub>, WS<sub>2</sub>, MoSe<sub>2</sub> and BN, are good candidates for codeposition with metal to form a super-hydrophobic composite coating. These substances are typical solid lubricants which are associated with the easy shearing of the weak interlayer (van der Waals) bonding. WS<sub>2</sub> is a promising lubricant for high temperature use, due to its thermal stability. In a previous study [10], the friction coefficient of the electrodeposited Ni coating against

mild steel was reduced from 0.8 to 0.5. In recent work, Zhao *et al.* [11] have successfully electrodeposited a super hydrophobic Ni-WS<sub>2</sub> coating showing excellent self-cleaning and corrosion resistant properties.

In the electrodeposition industry, Ni-P alloyed coatings have many possible advantages over other coatings including high hardness and wear resistance. They can be further heat treated producing a doubling of hardness, although their structure evolution between crystalline and amorphous forms can result in some challenges to co-deposition of Ni-P and WS<sub>2</sub> and thus few successful cases have been reported. Review of the literature shows some codeposition of Ni-P and WS<sub>2</sub> by electroless deposition reported [12, 13, 14]. In comparison to electroplating solutions, electroless deposition baths can be costly and have a limited lifetime. The operating conditions may include a high bath temperature. The present research focusses on the co-electrodeposition of Ni-P-WS<sub>2</sub> composite coatings followed by analysis of their properties especially in terms of self-lubrication and super-hydrophobicity. Surface roughness parameters were characterized and their relationship to the wetting behaviour were investigated.

## **2 Experimental details**

### **2.1 Coating deposition**

Ni-P-WS<sub>2</sub> composite coatings were deposited on a planar AISI 1020 mild steel substrate by one step electrodeposition without special equipment or rigorous condition restrictions. Before electrodeposition, the substrate was first ground using 120 and 800 grit silicon carbide papers to remove the surface oxide layer, then washed with detergents to remove any oil residue, and finally activated in 10 wt. % hydrochloric acid for 10 seconds and rinsed in

water to obtain an active fresh surface. The surface roughness (Ra) of the mild steel substrate after conditioning was approx. 3.4  $\mu\text{m}$ .

Electrodeposition was carried out in an aqueous electrolyte containing 220 g L<sup>-1</sup> NiSO<sub>4</sub>·6H<sub>2</sub>O, 30 g L<sup>-1</sup> H<sub>3</sub>BO<sub>3</sub>, 10 g L<sup>-1</sup> NaH<sub>2</sub>PO<sub>2</sub>, 12 g L<sup>-1</sup> HOC(COOH)(CH<sub>2</sub>COOH)<sub>2</sub> and 45 g L<sup>-1</sup> NiCl<sub>2</sub>·6H<sub>2</sub>O (Sigma-Aldrich). The concentration range of WS<sub>2</sub>, purchased from Shanghai ST-Nano Science & Technology, was 1-25 g L<sup>-1</sup> and cetyltrimethyl ammonium bromide (C<sub>16</sub>H<sub>33</sub>)N(CH<sub>3</sub>)<sub>3</sub>Br, CTAB) (Sigma-Aldrich) was added, as summarised in Table 1. All chemicals were added in sequence, with continuous stirring, until fully dissolved in solution. An ultrasonic cleaner, with an intensity of 1.3 W cm<sup>-2</sup>, was then deployed for 20 minutes to assist the dispersion of WS<sub>2</sub> nanoparticles. The Ni-P-WS<sub>2</sub> coating was electrodeposited at 60 °C for 45 minutes. The plating bath was maintained at a pH value of 2-3. The current density for Ni-P composite coating was 2.5 A dm<sup>-2</sup> as a higher current can induce network cracks [15]. The anode for electrodeposition was a pure Ni sheet (purity 99.5%) with a thickness of 1 mm, supplied by Goodman Alloys Ltd (Yorkshire, England). The cathode substrate was 3 mm thick AISI 1020 mild steel with a hardness of 120 HV. Both the anode and cathode were cut by a guillotine into rectangular plates of 80 mm × 10 mm. A PTFE-coated, cylindrical steel magnetic follower of 6 mm diameter and 25 mm length, centrally located at the bottom of an 80 mL cylindrical glass beaker, was rotated at 120 rev min<sup>-1</sup>. The vertically mounted, plane parallel electrodes of 4 cm<sup>2</sup> exposed area were immersed 25 mm apart in the bath.

## 2.2 Characterization of the coating

The surface morphologies of the coatings were observed using a scanning electron microscope (SEM) (JEOL JSM 6500F, Japan). The composition was determined using an energy dispersive spectrometer (EDS) in SEM. Stereoscopic 3D images of coating surfaces

with a pixel size of 0.2  $\mu\text{m}$  were constructed by a stand-alone software package MeX from the three tilted (+5 deg, 0 deg and -5 deg) secondary electron images (SEI). The coating was scratched into pieces and loaded into carbon-film copper grids of 3 mm in diameter for TEM observation. High resolution TEM (HRTEM) images were obtained from a JEOL JEM 3010 operating at 300 kV with a resolution of 0.21 nm. The crystalline phases of the coatings were examined using a Bruker D2 PHASER X-ray diffractometer with Cu-K $\alpha$  radiation, scanned at 0.02 deg  $\text{s}^{-1}$  in the 2 theta range from 10 deg to 80 deg. The hardness of the composite coatings was measured by a Vickers' microhardness instrument (Matsuzawa MHT-1) at an applied load of 100 g for 15 s. Reported values were averaged from 5 measurements.

Water contact angle measurements were obtained using a commercial instrument Drop Shape Analysis system (DSA100, Germany) with a computer-controlled liquid dispensing system. Distilled water droplets of 4  $\mu\text{L}$ . The values of WCA are averages of five measurements made on different areas of the surfaces. A reciprocating TE-77 tribometer (Phoenix, UK) was used to evaluate the friction behaviour in laboratory air with a relative humidity of 40-50% at 25 °C. The counter body was an AISI-52100 bearing steel ball (diameter 6 mm) with a hardness of 700 HV. The tests were carried out under a load of 14 N (initial Hertzian contact pressure of 1.6 GPa), a sliding frequency of 1 Hz and a sliding stroke of 2.69 mm. The frictional force was recorded automatically by a piezoelectric transducer.

### **3 Results and Discussion**

#### **3.1 Morphology and microstructure**

The as-received WS<sub>2</sub> powders were plates of 100-300 nm with the cross-section thickness at 50-70 nm as shown in Fig. 1a. Without particle embedment, the electrodeposited Ni-P coating presents a flat surface (Fig. 1b). In contrast, the composite Ni-P-WS<sub>2</sub> coating is quite rough, with clusters of protruding nodules on the surface (Fig. 1c). The TEM image in Fig.

1d) shows WS<sub>2</sub> particles in dark contrast are well embedded inside the Ni-P matrices. The selected area electron diffraction (SAED) pattern of this sample exhibits one bright and diffused ring which indicates the formation of small grains with the <111> Ni(P) textures. The EDS spectrum in Fig. 1(e) exhibits that the coating primarily consists of the four elements: Ni, P, W and S, indicating the embedment of WS<sub>2</sub> particles into the coating by codeposition.

XRD patterns in Fig. 1(f) show three XRD of WS<sub>2</sub> powders, Ni-P and Ni-P-WS<sub>2</sub> coating corresponding to Figs. 1 (a-c) respectively. The XRD peaks from the as received WS<sub>2</sub> powders are consistent with the standard non-texture WS<sub>2</sub>. Both Ni-P coating and Ni-P-WS<sub>2</sub> composite coating had a broad peak at 45° which was consistent with {111} planes of nickel. This strong peak on {111} indicated the Ni(P) nucleated and grew along the coating surface thus as a result formed a relatively smooth surface. Neglecting internal stress, the grain sizes were calculated using the Scherrer equation to range from 2.7 nm in Ni-P to 1.5 nm in Ni-P-WS<sub>2</sub>. As the growth of the electrodeposited layer consists of both nucleation and crystal growth, there is a competition between these two processes. The addition of WS<sub>2</sub> particles provides more sites for nucleation and retards the growth of crystals, producing a smaller grain size. The remaining peaks in the Ni-P-WS<sub>2</sub> coating at 14 deg, 33 deg, 34 deg, 40 deg, 49 deg, 58 deg, 60 deg and 61 deg are in accordance with the (002), (100), (102), (103), (106), (110), (008) and (112) peaks of hexagonal WS<sub>2</sub>. By applying the Scherrer equation to the strong (002) peak, the averaged crystallite size of the WS<sub>2</sub> in coating is calculated to be 14 nm which is much lower than the crystallite size of the as-received WS<sub>2</sub> particles. This discrepancy could be due to the fact that particles with smaller sizes may have a higher probability of suspension and hence adhesion onto the electrode surface during codeposition.

### 3.2 Effect of WS<sub>2</sub> concentration

The stability of the 15 g L<sup>-1</sup> WS<sub>2</sub> bath was evaluated by a sedimentation test. The WS<sub>2</sub> particles in the bath without surfactant settled quickly once magnetic stirring stopped, resulting in a sediment height below 50% and clear supernatant within 5 min. In contrast, the well-dispersed WS<sub>2</sub> particles in the bath with 0.1 g L<sup>-1</sup> CTAB sedimented very slowly, showing prolonged stability for 1 hour. Moreover, the CTAB containing bath could be redispersed as a sol by magnetic stirring, whereas the bath without surfactant proved difficult to re-disperse by magnetic stirring. In another composite electrodeposition system [16], the addition of 0.2 g L<sup>-1</sup> of CTAB was found to shift the zeta potential of particles to + 5.5 mV, i.e., a small positive surface charge was experienced due to adsorption of the cationic surfactant.

Different surface morphologies were fabricated by varying the WS<sub>2</sub> and CTAB concentrations in the basic plating solution. The Ni-P-WS<sub>2</sub> coating deposited at 1 g L<sup>-1</sup> of WS<sub>2</sub> and 0.1 g L<sup>-1</sup> of CTAB presents a rough morphology containing many round nodule-like protrusions with an average diameter of around 5 µm (Fig. 2a). As the concentrations of WS<sub>2</sub> and CTAB increase, both the height and base radius of these protrusions increase as shown in Fig. 2b. On further increase of WS<sub>2</sub> concentration, these protrusions started to show a “broccoli-like” appearance, which is several tens of micrometres in diameter and consists of densely packed submicron-sized bumps in Fig. 2c)-f). Cross-sectional SEM images in Fig. 3 a)-f) show that the thickness of the composite coating increased from 20 µm to 40 µm as the particle concentration in the bath was raised from 1 g L<sup>-1</sup> to 25 g L<sup>-1</sup>. Back scattered electron (BSE) images in Fig. 3 g)-h) confirm that many WS<sub>2</sub> particles were entrapped and uniformly dispersed inside the coating.

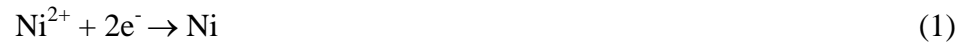
As illustrated in Fig. 4a), the WS<sub>2</sub> amounts incorporated in the coatings have an almost linear increase with their concentrations up to 15 g L<sup>-1</sup> in the baths. A further increase of WS<sub>2</sub> concentration to 25 g L<sup>-1</sup>, however, resulted in a decrease of WS<sub>2</sub> content in the coating. This could be due to a high concentration of WS<sub>2</sub> causing aggregation of particles which then drop to the bottom of the electrolytic cell. As a typical cationic surfactant, CTAB is a long chain molecule with a positively-charged hydrophilic head and uncharged, hydrophobic tail [17,18]. The head chain helps to disperse particles and avoid agglomeration, while the tail chemistry can charge the suspended particles positively by electrostatic adsorption, resulting in strong attraction of the modified particles to the cathode surface and effective codeposition of Ni-P and WS<sub>2</sub> on the surface via electrophoresis. Excessively high concentration of CTAB in solution however may occupy numerous nucleation sites and thus block the deposition of WS<sub>2</sub> particles.

Fig. 4b) shows that the hardness of the composite coatings increases with the incorporation of nano-size WS<sub>2</sub> particles. The composite coating with the highest WS<sub>2</sub> content has a peak hardness of 720 ± 50 HV. The increased hardness is mainly attributable to the reduction of grain size after the addition of WS<sub>2</sub> and CTAB [19]. A high content of incorporated WS<sub>2</sub> nanoparticles is also desirable to significantly hinder dislocation motion via dispersion hardening.



### 3.3 Mechanism of deposition and hierarchical coating growth

The main cathodic reaction during electrodeposition is reduction of nickel ions to nickel metal:



Hydrogen evolution occurs as a secondary reaction:



Reduction of hypophosphite ion at the cathode leads to phosphorus being codeposited with nickel [20]:



A simplified mechanism for formation of the Ni-P coating is shown in Fig. 5a). A homogenous Ni-P solid solution coating can be produced. For the Ni-P-WS<sub>2</sub> composite coatings, WS<sub>2</sub> adsorbs the CTAB surfactant and its quaternary ammonium groups (-NH<sub>4</sub><sup>+</sup>) provide a positive surface charge. WS<sub>2</sub> is transported to the cathode by both convective-diffusion and electrophoretic migration of the positively charged particles. The incorporation of WS<sub>2</sub> particles into the Ni-P electrodeposit was found to cause significant change of surface morphology from: (1) a planar smooth surface, to (2) a nodular rough surface and then to (3) a hierarchical rough surface. The growth of these nodule and hierarchical ‘broccoli-like’ structures could be explained by the redistribution of currents on the electrode surface by conductive WS<sub>2</sub> particles P [21]. As shown in Fig. 5b), the WS<sub>2</sub> particles adhered to the cathode will change the electric field, with a higher current density on particles than the surrounding area. The Ni-P deposits will prefer to grow on the top of WS<sub>2</sub> particles as the higher current density leads to more active reduction of nickel ions [22]. This results in

numerous nodular structures followed by overlapping to form the hierarchical ‘broccoli-like’ structures in Fig. 5c).

### **3.4 Hydrophobicity**

The wettability of Ni-P and Ni-P-WS<sub>2</sub> coatings has been evaluated by water contact angle measurements without any pretreatment. Fig. 6 shows the variation of contact angles as a function of the WS<sub>2</sub> contents in the corresponding coatings. Without WS<sub>2</sub> the Ni-P coating shows the lowest WCA of 87 deg. As the WS<sub>2</sub> content increased to 1.3 wt% the WCA increased to 131 deg. This indicates that the nodular structures partially prevent the direct contact of water droplets with the matrix deposit. Super-hydrophobicity can be found in the coatings with WS<sub>2</sub> over 3.6 wt%. The 4.8 wt% WS<sub>2</sub> coating shows the highest contact angle of 157 deg. This is due to the hierarchical surface structure which combines both microscale and submicron-sized roughness. In such a hierarchical structure, air is easily trapped in the dual scale structure to prevent direct contact. The super-hydrophobicity of the as-prepared coatings remained after twelve months exposure in air.

### **3.5 The influence of roughness on WCA**

This study shows that the surface roughness significantly affects the wettability behaviour. 3D surface reconstruction of the coating in Fig. 7 shows that the composite coating deposited in the electrolyte with 1 g L<sup>-1</sup> WS<sub>2</sub> concentration presents a uniform contrast, suggesting a flat surface. With the increase of WS<sub>2</sub> concentrations up to 15 g L<sup>-1</sup>, the composite surfaces show the highest contrast (orange/purple colours) indicating larger height and size of the

protrusions. On further increase of the  $\text{WS}_2$  concentration to  $25 \text{ g L}^{-1}$ , the green/purple contrast colours now indicate a reduced surface roughness due to the overlap of protrusions.

Four common surface roughness parameters were characterized from these 3D models (Table 2) and their variation with WCA is shown in Fig. 8. The roughness average ( $R_a$ ), defined as the arithmetical mean deviation of the roughness profiles, is most commonly used to evaluate surface roughness. Fig. 8a) shows that the hydrophobicity (WCA) increases with  $R_a$  values of the surface. At roughnesses ( $R_a$ ) higher than  $6.36 \text{ }\mu\text{m}$ , superhydrophobic (WCA  $>150 \text{ deg}$ ) coatings were formed. WCA was also plotted against the mean height of the roughness profile elements ( $R_c$ ). As shown in Fig. 8b), an increase of  $R_c$  over the range of  $0\text{-}20 \text{ }\mu\text{m}$  leads to significant increase of WCA, indicating that the protrusion height is an important factor affecting hydrophobicity. The mean width roughness ( $R_{Sm}$ ) shows that the coating with sparsely scattered protrusions (high  $R_{Sm}$ ) has a lower WCA in Fig. 8c). Another important profile parameter is skewness of roughness ( $R_{sk}$ ) which describes the shapes of peaks and valleys.  $R_{sk} < 0$  corresponds to valley dominance, and  $R_{sk} > 0$  corresponds to peak dominance. The relationship between  $R_{sk}$  and WCA in Fig. 8d) shows that super-hydrophobicity occurs when the absolute  $R_{sk}$  was less than 0.5. It has also been argued in [23,24] that a symmetrical distribution of peaks and valleys (i.e.  $R_{sk}$  close to 0) will enhance super hydrophobicity.

### 3.6 Hydrophobicity mechanism

The wetting behaviour of droplets on the surfaces can be explained by either Wenzel's model [25] or Cassie-Baxter's model [26]. Wenzel's model was developed to describe the wettability of a surface that is totally wetted by the liquid, and where no air is trapped between the liquid and the solid surface. The apparent contact angle  $\theta$  is considered to be a function of  $r$ :

$$\cos\theta = r \cos\theta_y \quad (4)$$

where  $r$  is the dimensionless roughness, defined as the ratio of the true area of the surface to its projected area on the horizontal and  $\theta_y$  represents the static contact angle on the smooth surface. This equation suggests that when  $\theta_y > 90$  deg the water repellence increases with  $r$ ; where  $\theta_y < 90$  deg,  $\theta$  decreases with  $r$ .

The Cassie-Baxter model predicts the wetting of a surface where air is trapped between the liquid and the solid to support a droplet. In this model, roughness can reduce apparent surface wettability regardless of the intrinsic wettability behaviour of the base material. This wetting behaviour can be described by the following equation:

$$\cos\theta = f_{SL} \cos\theta_y + f_{LA} \cos\theta_A \quad (5)$$

where  $\theta$  represents the contact angle on a heterogeneous surface composed of a solid and air,  $\theta_A$  is the contact angle of a droplet with the gas phase and can be considered up to 180 deg,  $f_{SL}$  and  $f_{LA}$  are the area fractions of solid and air in contact with liquid. The sum of  $f_{SL}$  and  $f_{LA}$  is unity if the droplet is small enough to neglect sagging and Laplace pressure is constant between the high curvature front and the smaller curvature rear [27].

The Ni-P surface has a water contact angle of 87 deg and is intrinsically hydrophilic [28]. With increasing surface roughness of the electrodeposited Ni-P-WS<sub>2</sub> coating, the contact angles should decrease according to Wenzel's formulation, which is contrary to the observed WCA increase in Fig. 6. It is thought that the rough surfaces of the Ni-P-WS<sub>2</sub> deposits allow

a water droplet to partially sit on the air pockets between protrusions, maintaining the hydrophobic Cassie-Baxter state as illustrated in Fig. 9. The area fractions of the air-droplet contact on the different Ni-P-WS<sub>2</sub> coatings were calculated using the Cassie-Baxter equation and are listed in Table 3. The  $f_{LA}$  value increased from 28.35% on nodular roughness to 92.27% on hierarchical surface. The micron-sized broccoli-like protrusions combined submicron-sized particles and cavities which could accommodate a large fraction of air therefore resulting in excellent water repellence properties, the highest WCA being 157 deg, as shown in Fig. 6.

### 3.7 Friction and wear testing

Fig. 10 shows how the coefficients of friction (CoF) changed during wear tests for the different levels of WS<sub>2</sub> containing coatings. All the coatings started with a CoF around 0.2. For the coatings with low WS<sub>2</sub> of 0.5 wt%, and 1.3 wt%, the CoF rapidly increased then stabilised at 0.7-0.8. The results indicate that the lubricating WS<sub>2</sub> was effective initially but gradually lost function during the wear process. For the 2.3 wt% WS<sub>2</sub> coating, the CoF was maintained for up to 400 seconds in the sliding wear test and then increased gradually. In contrast, for the composite coatings with 3.6 wt% WS<sub>2</sub> and above, the CoF exhibited a stable response at 0.17-0.2 during whole friction test, much lower than the friction coefficient of Ni-P (0.5). This significant friction reduction is due to the low shear yield of the WS<sub>2</sub> and its high abundance which can consistently provide a lubrication function for a long period. One of the main tribological properties of rubbed pairs is self-lubrication. The key to self-lubricating materials is the rapid and easy shear and transfer of thin films from one surface to another. The wear track depth was measured to evaluate the wear degree of coatings. As shown in Fig. 11, the depth of the wear track formed on Ni-P-WS<sub>2</sub> increased as the content of

WS<sub>2</sub> was raised from 0.5 wt% to 2.3 wt%. This can be attributed to the increased surface roughness and coating thickness as shown in Fig. 3. High particle contents over 3.6 wt% in the coatings resulted in a shallow wear track, which is related to the low friction coefficient, < 0.2.

The corresponding wear tracks were imaged in the SEM as shown in Fig. 12. The Ni-P-WS<sub>2</sub> (0.5 wt%) coating has the widest wear track width of 450 μm. The observed grooves and scars along the sliding direction indicate that severe adhesive wear occurred. As the WS<sub>2</sub> content in the samples increased, the wear tracks had defined narrower widths and the Ni-P-WS<sub>2</sub> 4.8 wt% sample exhibits the narrowest wear track of 260 μm. These wear tracks had much less debris, which reflected their improved wear resistance.

The worn areas of the counterpart balls after the friction testing were also examined as shown in Fig. 13. The counterpart balls tested against the 0.5 and 2.3 wt% WS<sub>2</sub> coating exhibits a rough wear scar surrounded by widely spread pieces of debris in Figs. 12a) and b). The counterpart balls tested against the increased WS<sub>2</sub> content composite coatings resulted in far less debris on/around the wear scar, as shown in Figs. 12c) and d). There was only a tiny wear scar on the ball after sliding against 4.8 wt% WS<sub>2</sub> coating having the lowest percentage of oxygen (Table 4). A sufficient WS<sub>2</sub> particle content in the coatings will ensure a complete tribofilm is formed to prevent coating/steel contact, reducing wear damage and oxidation [22].

## 4 Conclusions

Ni-P-WS<sub>2</sub> coatings having combined super-hydrophobic and self-lubricating properties have been achieved by a simple electrochemical deposition route combining electroplating of metal with electrophoretic deposition of a solid lubricant. The surface morphology and wetting ability were investigated with varied particle and surfactant concentrations in the electrolyte. The Ni-P composite coatings with 2.3 wt.% of WS<sub>2</sub> or more were observed to have microscale broccoli-like protrusions composed of submicron-sized papillae with the highest WCA of 157 deg. The Ni-P-WS<sub>2</sub> coatings also exhibit self-lubricating performance in the reciprocal sliding test against steel balls. Sufficient WS<sub>2</sub> in the composite coating will ensure the formation of a uniform tribofilm to keep a low coefficient of friction (as low as 0.17). This one-step electrodeposition, with the advantages of low cost, simple equipment and repeatable process, may provide an effective approach towards the production/fabrication of liquid repellent and low friction surfaces for a variety of applications, such as oil-water separation, train and car drive train components and wind turbine blades.

## Acknowledgments

We would like to acknowledge financial supports from China Scholarship Council (CSC), Faculty of Engineering and the Environment at University of Southampton, Royal Society International Exchanges Scheme (IE151191), and EPSRC Global Challenge Research Fund.

**Table 1 Concentrations of WS<sub>2</sub> and CTAB used to electrodeposit Ni-P-WS<sub>2</sub> coatings.**

| Sample  | a   | b   | c   | d   | e   | f   |
|---|-----|-----|-----|-----|-----|-----|
| WS <sub>2</sub> particles / g L <sup>-1</sup> | 1   | 3   | 7   | 10  | 15  | 25  |
| CTAB / g L <sup>-1</sup>                      | 0.1 | 0.1 | 0.1 | 0.2 | 0.2 | 0.3 |

**Table 2 Roughness average ( $R_a$ ), mean height ( $R_c$ ), mean spacing ( $R_{Sm}$ ) and skewness ( $R_{sk}$ ) of the roughness profile elements of the electrodeposited Ni-P-WS<sub>2</sub> coatings.**

| Sample | $R_a$ / $\mu$ m | $R_c$ / $\mu$ m | $R_{Sm}$ / $\mu$ m | $R_{sk}$ | WCA /deg |
|--------|-----------------|-----------------|--------------------|----------|----------|
| Ni-P   | –               | –               | –                  | –        | 87       |
| a      | 0.70            | 8.46            | 212.58             | 1.42     | 101      |
| b      | 2.40            | 10.13           | 133.23             | 1.73     | 131      |
| c      | 5.77            | 18.60           | 127.48             | 0.87     | 147      |
| d      | 6.36            | 19.90           | 103.35             | 0.51     | 154      |
| e      | 9.61            | 30.46           | 111.73             | -0.26    | 157      |
| f      | 7.25            | 20.97           | 102.78             | -0.47    | 152      |

**Table 3 Fraction of solid-liquid interface ( $f_{SL}$ ) and liquid-air interface ( $f_{LA}$ ) in a plane geometrical contact area for the electrodeposited Ni-P-WS<sub>2</sub> coatings.**

| Sample | Water contact angle /deg | % $f_{SL}$ | % $f_{LA}$ |
|--------|--------------------------|------------|------------|
| Ni-P   | 87                       | -          | -          |
| a      | 101                      | 71.65      | 28.35      |
| b      | 131                      | 32.03      | 67.97      |
| c      | 147                      | 15.65      | 84.35      |
| d      | 154                      | 9.83       | 90.17      |
| e      | 157                      | 7.73       | 92.27      |
| f      | 152                      | 11.36      | 88.64      |



Table 4 EDS comparison of the whole wear scars on counterpart balls after wear test against different Ni-P-WS<sub>2</sub> coatings.

| Counterpart<br>Coating (wt%) | Ni  | P   | S   | W   | Cr  | Fe   | O K |
|------------------------------|-----|-----|-----|-----|-----|------|-----|
| Vs. NiP-0.5WS <sub>2</sub>   | 0.2 | -   | 0.1 | 0.2 | 1.5 | 90.5 | 7.5 |
| Vs. NiP-2.3WS <sub>2</sub>   | 4.4 | 0.7 | 0.1 | 0.3 | 1.5 | 88.6 | 4.4 |
| Vs. NiP-3.6WS <sub>2</sub>   | 7.2 | 0.7 | 0.1 | 0.4 | 1.4 | 87.3 | 2.9 |
| Vs. NiP-4.8WS <sub>2</sub>   | 2.6 | 0.4 | 0.2 | 0.9 | 1.5 | 91.6 | 2.8 |

## Figure captions

Fig. 1 a) An SEM image of as-received WS<sub>2</sub> nanoparticles, b) An SEM image of Ni-P coating, c) An SEM image, d) A TEM image, e) An EDS spectrum and (f) XRD patterns of the Ni-P-WS<sub>2</sub> coating prepared in an electrolyte containing 15 g L<sup>-1</sup> WS<sub>2</sub> ( $T = 60\text{ }^{\circ}\text{C}$ ,  $t = 45\text{ min}$ ,  $j = 2.5\text{ A dm}^{-2}$ ). The inset shows an SAED pattern of the whole area in d).

Fig. 2 (a-f) SEM images for Ni-P-WS<sub>2</sub> coatings deposited at WS<sub>2</sub> concentrations of 1, 3, 7, 10, 15 and 25 g L<sup>-1</sup> in chronological letter order ( $T = 60\text{ }^{\circ}\text{C}$ ,  $t = 45\text{ min}$ ,  $j = 2.5\text{ A dm}^{-2}$ ) and the insets show high magnification images of protrusions in a)-f) with the yellow scale bar representing a length of 1  $\mu\text{m}$ .

Fig. 3 (a-f) Cross-sectional SEM images of Ni-P-WS<sub>2</sub> coatings deposited at WS<sub>2</sub> concentrations of 1, 3, 7, 10, 15 and 25 g L<sup>-1</sup> in chronological letter order, and g)-h) Cross-sectional BSE images of Ni-P-WS<sub>2</sub> coatings deposited at 3 g L<sup>-1</sup>.

Fig. 4 (a) The content of WS<sub>2</sub> in the coating as a function of the concentration of WS<sub>2</sub> particles in the electrolyte and b) the Vickers hardness of coating as a function of the content of WS<sub>2</sub> in coating.

Fig. 5 Schematic illustration of the growth process of a) Ni-P coating, b) Ni-P-WS<sub>2</sub> at a low WS<sub>2</sub> concentration and c) Ni-P-WS<sub>2</sub> at a high WS<sub>2</sub> concentration.

Fig. 6 Contact angle of the electrodeposited coatings as a function of the WS<sub>2</sub> content of the coating.

Fig. 7 (a-f) Stereoscopic images of the Ni-P-WS<sub>2</sub> coatings deposited at WS<sub>2</sub> concentrations of 1, 3, 7, 10, 15 and 25 g L<sup>-1</sup> respectively. The inset scale bar represents the length of 50  $\mu\text{m}$  and is applicable to all images.

Fig. 8 Relationship between WCA and surface roughness parameters ( $R_a$ ,  $R_c$ ,  $R_{Sm}$ ,  $R_{sk}$ ) for different Ni-P-WS<sub>2</sub> coatings.

Fig. 9 Schematic of water droplet on different coating surfaces.

Fig. 10 Coefficient of friction as a function of time for the electrodeposited coatings of different WS<sub>2</sub> content.

Fig. 11 Surface profiles of the wear tracks formed in the electrodeposited coatings having different WS<sub>2</sub> contents.

Fig. 12 Comparison of wear tracks for different coatings: a) 0.5 wt% WS<sub>2</sub>, b) 2.3 wt% WS<sub>2</sub>, c) 3.6 wt% WS<sub>2</sub>, and d) 4.8 wt% WS<sub>2</sub>.

Fig. 13 Surface morphologies of counterpart balls after 1000 s friction test against different Ni-P-WS<sub>2</sub> coatings: (a) 0.5 wt% WS<sub>2</sub>, b) 2.3 wt% WS<sub>2</sub>, c) 3.6 wt% WS<sub>2</sub>, and d) 4.8 wt% WS<sub>2</sub>.

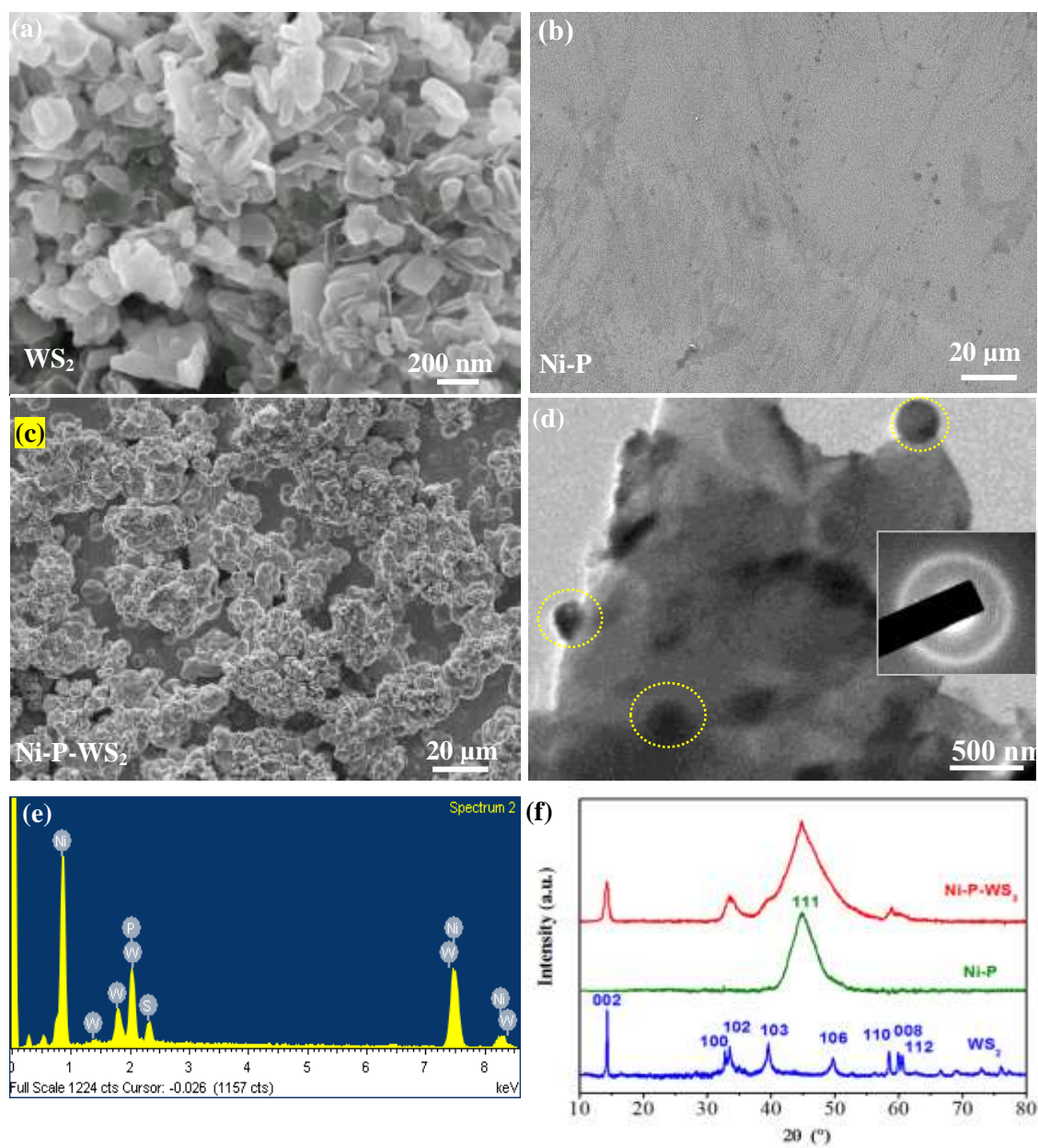
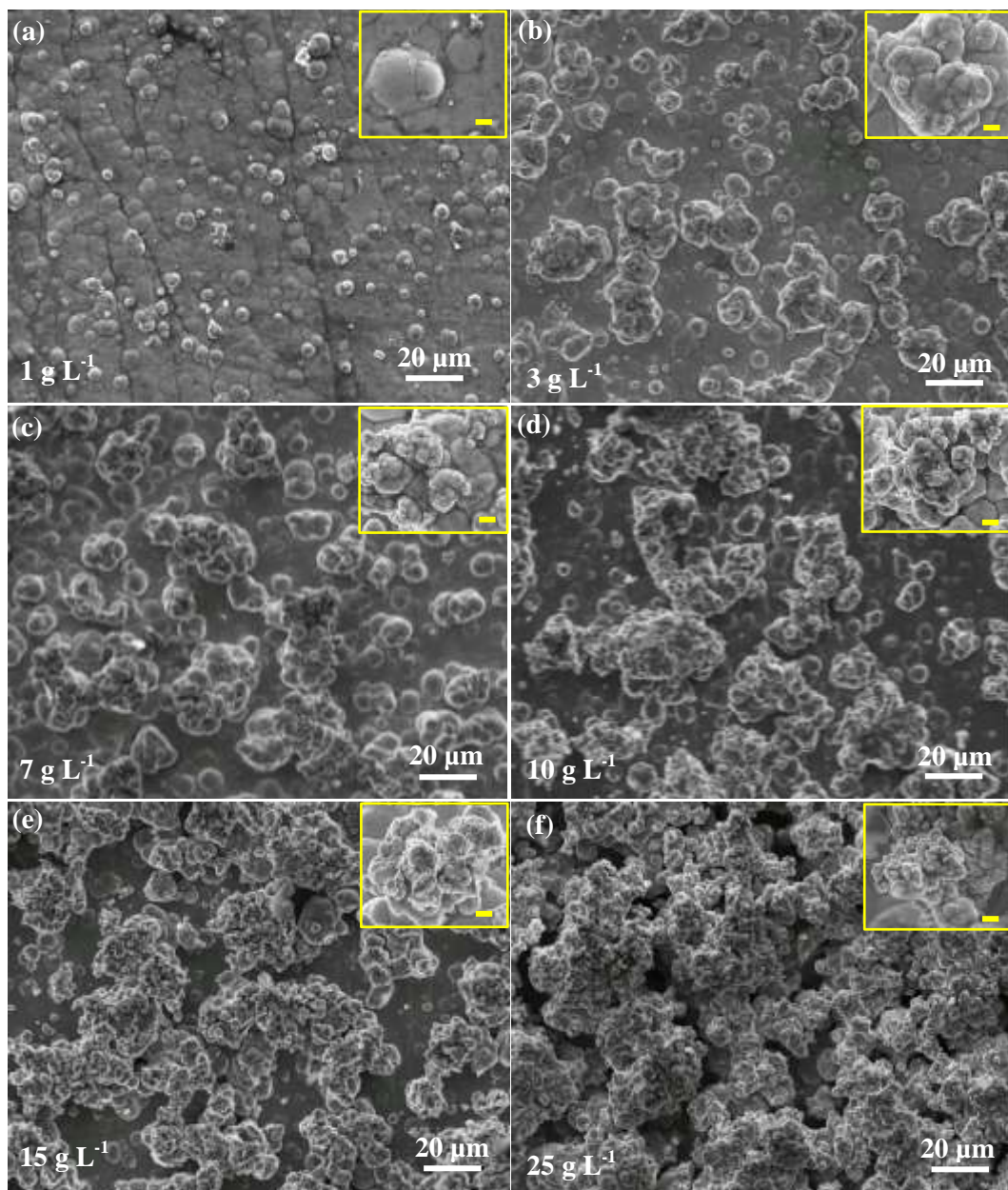


Fig. 1



**Fig. 2**

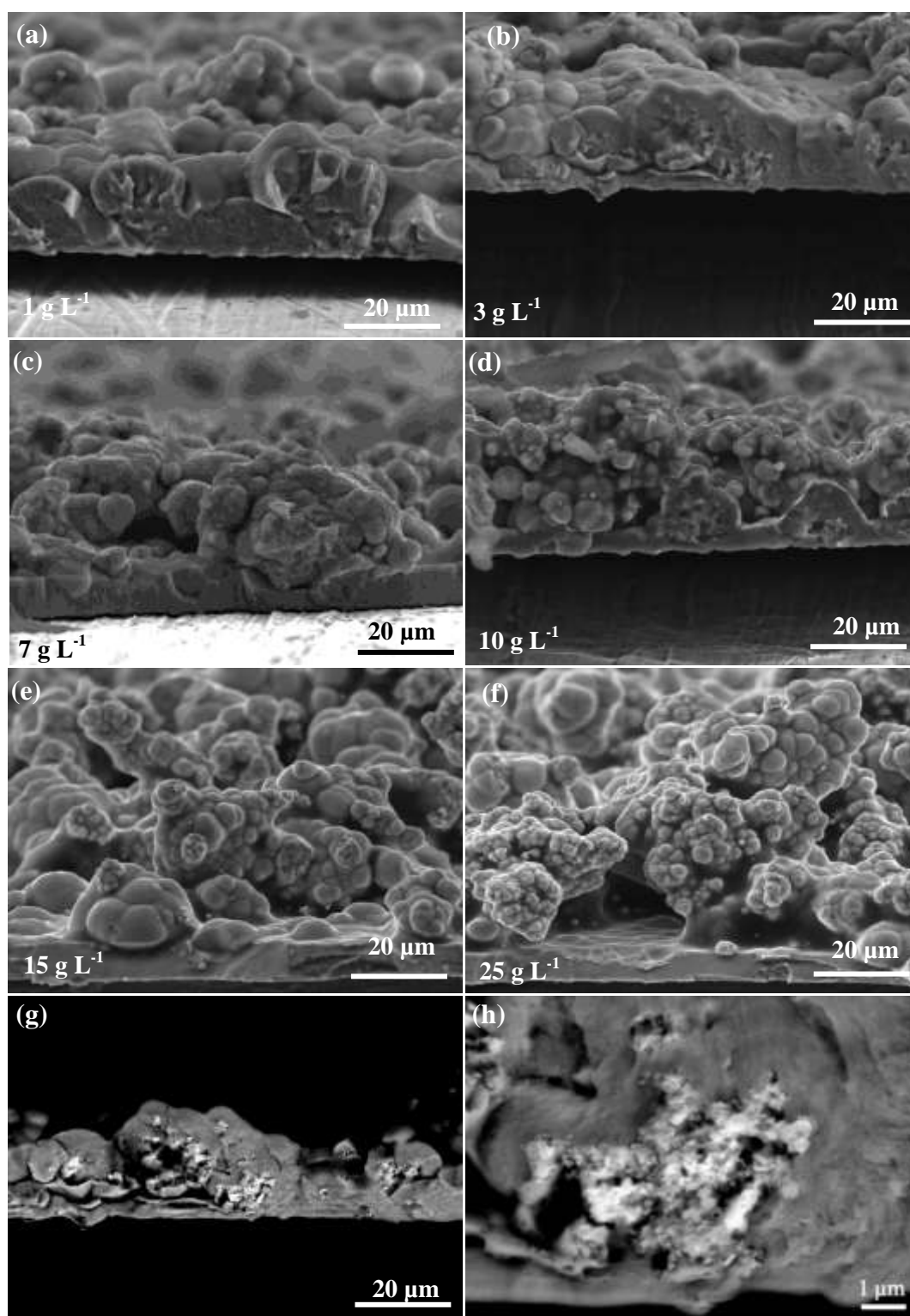
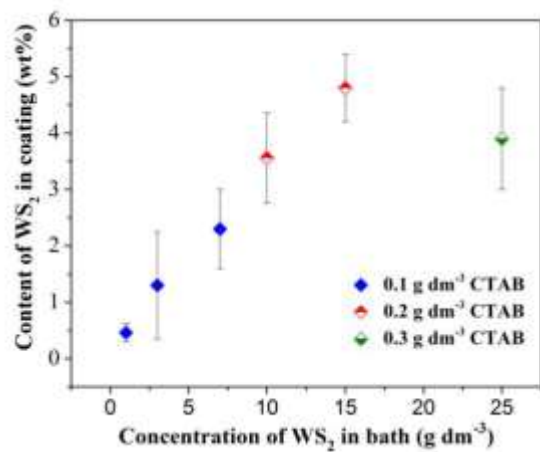
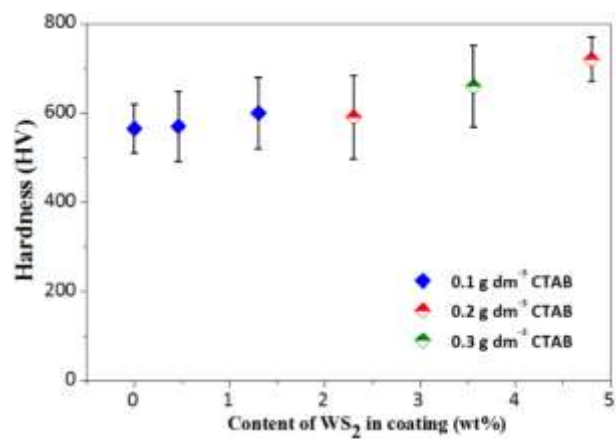


Fig. 3

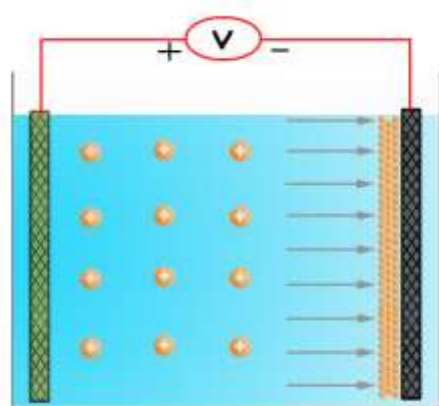


(a)

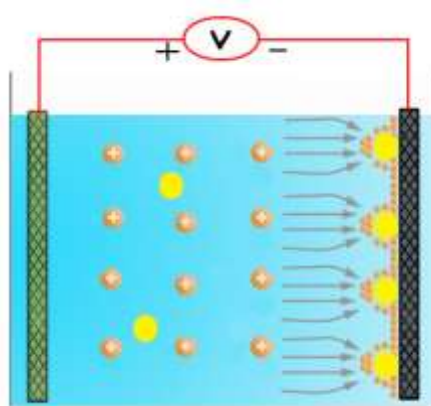


(b)

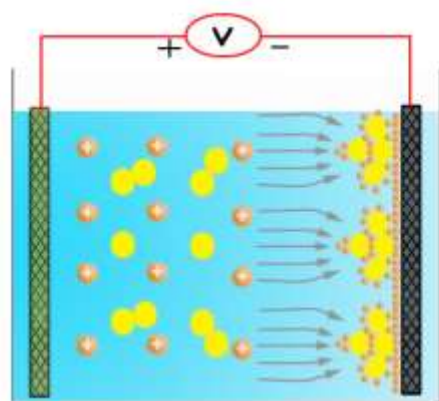
Fig. 4



(a)



(b)



(c)



 Ni-P deposit  
  $WS_2$  particle

Fig. 5



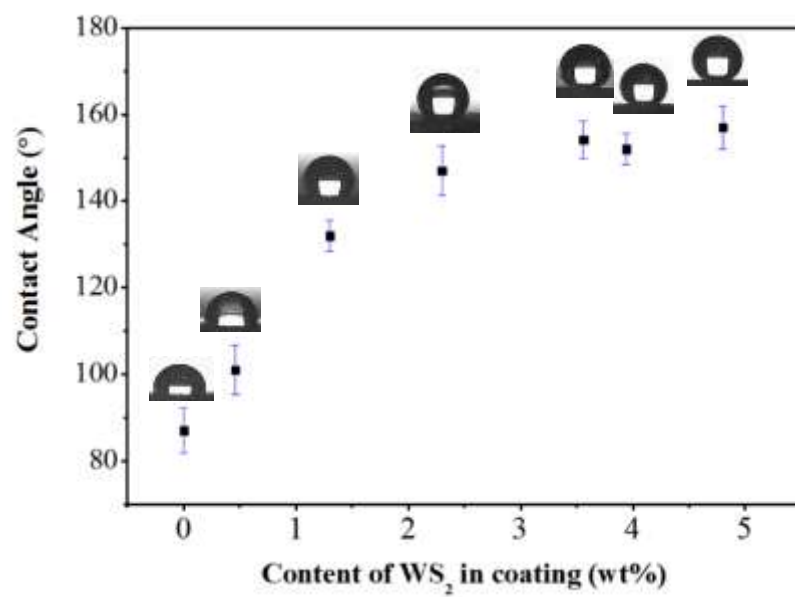


Fig. 6

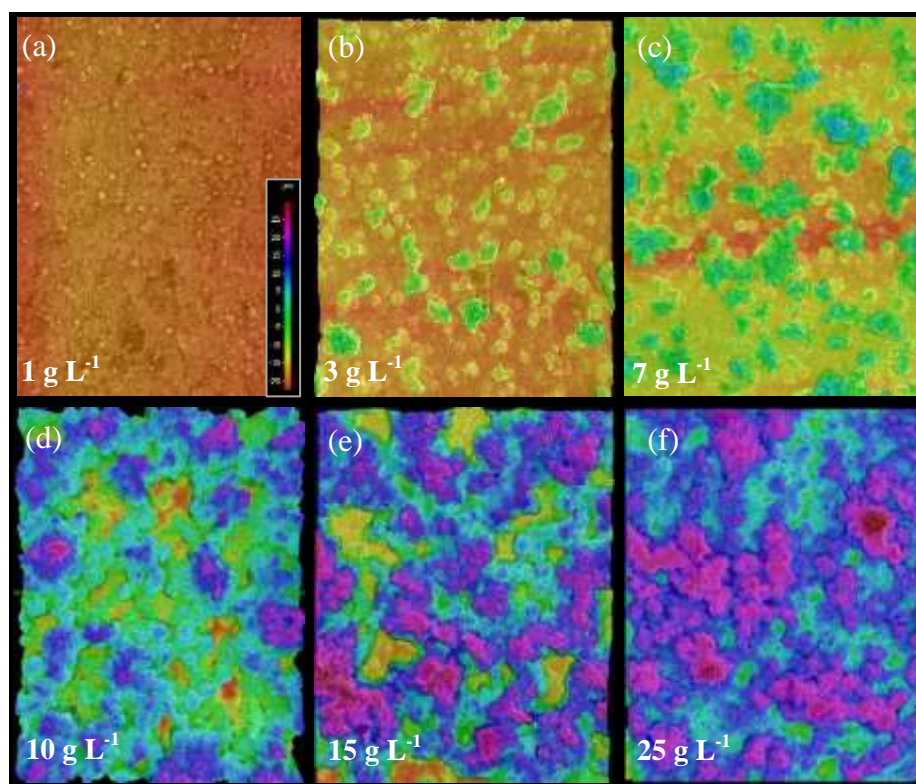


Fig. 7



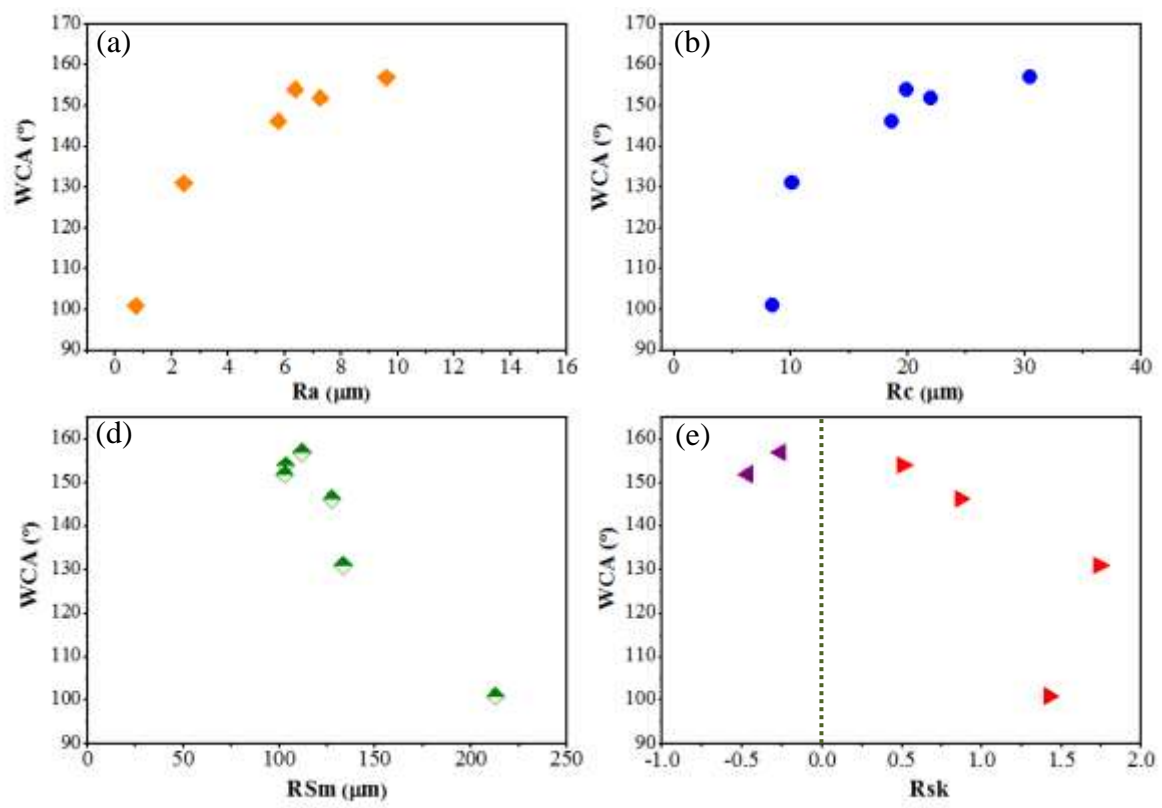


Fig. 8

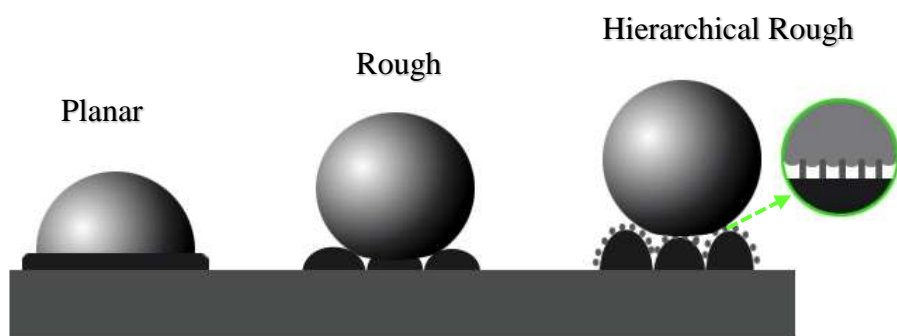


Fig. 9

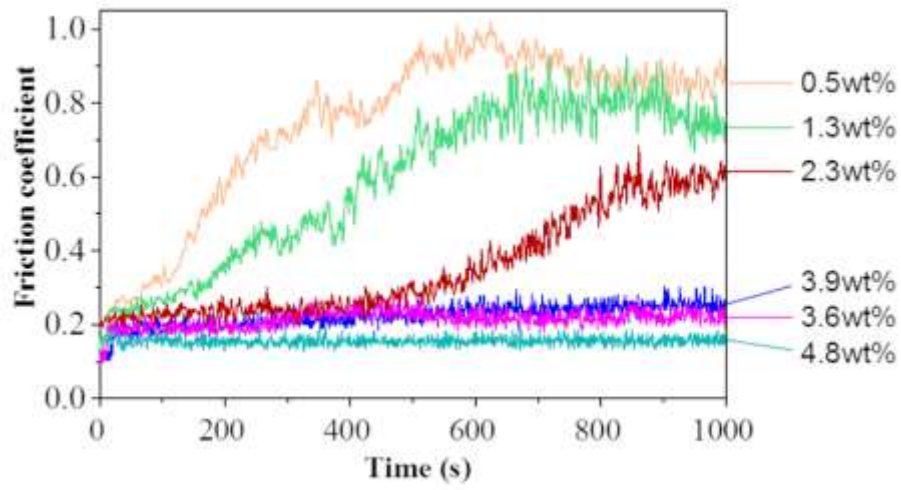


Fig. 10

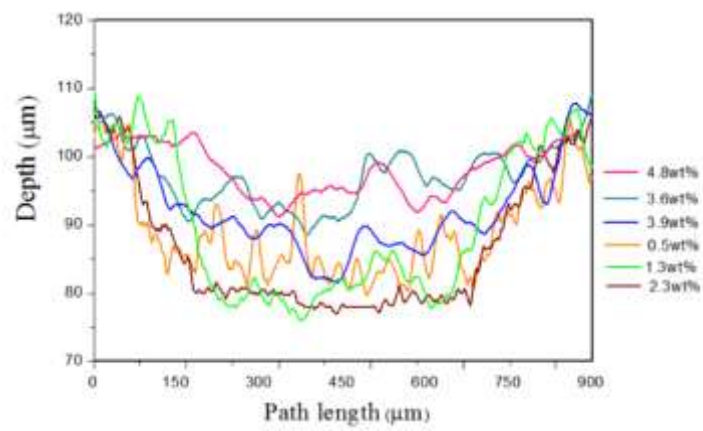
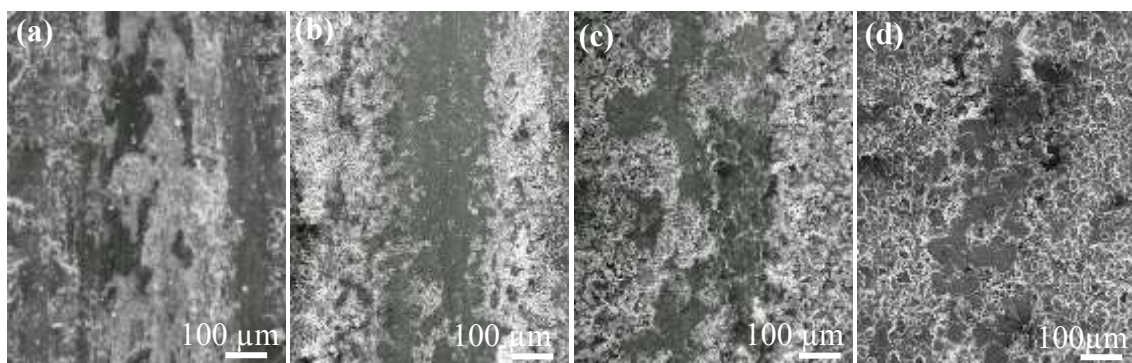
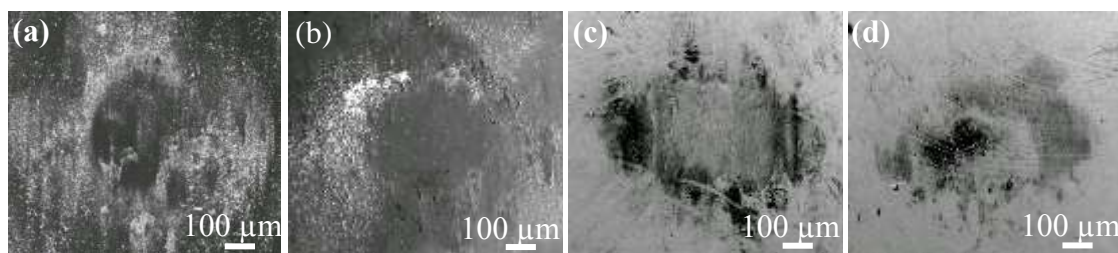


Fig. 11



**Fig. 12**



**Fig. 13**

## References

- 
- <sup>1</sup> T. Sun, G. Wang, F. Lin, B. Liu, Y. Ma, J. Lei, D. Zhu, Reversible switching between superhydrophilicity and superhydrophobicity, *Angewandte Chemie International Edition* 116 (2004) 361-364.
- <sup>2</sup> T. Darmanin, E.T. de Givenchy, S. Amigoni, F. Guittard, Superhydrophobic surfaces by electrochemical processes, *Advanced Materials* 25 (2013) 1378-1394.
- <sup>3</sup> M. Shafiei, A.T. Alpas, Nanocrystalline nickel films with lotus leaf texture for superhydrophobic and low friction surfaces, *Applied Surface Science* 256 (2009) 710-719.
- <sup>4</sup> W. Geng, A. Hu, M. Li, Super-hydrophilicity to super-hydrophobicity transition of a surface with Ni micro–nano cones array, *Applied Surface Science* 263 (2012) 821-824.
- <sup>5</sup> H. Xiao, A. Hu, T. Hang, M. Li, Electrodeposited nanostructured cobalt film and its dual modulation of both superhydrophobic property and adhesiveness, *Applied Surface Science* 324 (2015) 319-323.
- <sup>6</sup> N.J. Shirtcliffe, G. Mchale, C.C. Perry, Wetting and wetting transitions on copper-based superhydrophobic surfaces, *Langmuir the Acs Journal of Surfaces & Colloids* 21 (2005) 937-943.
- <sup>7</sup> B. Zhang, X. Zhao, Y. Li, B. Hou, Fabrication of durable anticorrosion superhydrophobic surfaces on aluminum substrates via a facile one-step electrodeposition approach, *Rsc Advances* 6 (2016) 35455-35465.
- <sup>8</sup> S. Huang, Y. Hu, W. Pan, Relationship between the structure and hydrophobic performance of Ni–TiO<sub>2</sub> nanocomposite coatings by electrodeposition, *Surface & Coatings Technology* 205 (2011) 3872-76.
- <sup>9</sup> J.M. Lee, M.B. Kong, K.K. Jung, H.J. Ji, J.S. Ko, Creation of microstructured surfaces using Cu–Ni composite electrodeposition and their application to superhydrophobic surfaces, *Applied Surface Science* 289 (2014) 14-20.
- <sup>10</sup> E. García-Lecina, I. García-Urrutia, J.A. Díez, J. Fornell, E. Pellicer, J. Sort, Codeposition of inorganic fullerene-like WS<sub>2</sub> nanoparticles in an electrodeposited nickel matrix under the influence of ultrasonic agitation, *Electrochimica Acta* 114 (2013) 859-867.
- <sup>11</sup> G. Zhao, Y. Xue, Y. Huang, Y. Ye, F.C. Walsh, J. Chen, S.C. Wang, One-step electrodeposition of a self-cleaning and corrosion resistant Ni/WS<sub>2</sub> superhydrophobic surface, *RSC Advances* 6 (2016) 59104-59112.

- 
- <sup>12</sup> A. Katz, M. Redlich, L. Rapoport, H.D. Wagner, R. Tenne, Self-lubricating coatings containing fullerene-like WS<sub>2</sub> nanoparticles for orthodontic wires and other possible medical applications, *Tribology Letters* 21 (2006) 135-139.
- <sup>13</sup> W.X. Chen, J.P. Tu, Z.D. Xu, R. Tenne, R. Rosenstveig, W.L. Chen, H.Y. Gan, Wear and friction of ni-p electroless composite coating including inorganic fullerene-WS<sub>2</sub> nanoparticles, *Advanced Engineering Materials* 4 (2002) 686-690.
- <sup>14</sup> I. Sivandipoor, F. Ashrafizadeh, Synthesis and tribological behaviour of electroless Ni-P-WS<sub>2</sub> composite coatings, *Applied Surface Science* 263 (2012) 314-319.
- <sup>15</sup> Y. He, Electrodeposition of nickel-based composite coatings for tribological applications, PhD thesis, University of Southampton, December 2015.
- <sup>16</sup> S. Ranganatha, T.V. Venkatesha, K. Vathsala. Electrochemical studies on Zn/nano-CeO<sub>2</sub> electrodeposited composite coatings, *Surface & Coatings Technology* 208 (2012) 64-72.
- <sup>17</sup> Y. He, S.C. Wang, F.C. Walsh, W. Li, L. He, P.A. Reed, The monitoring of coating health by in-situ luminescent layers, *RSC Advances* 5 (2015) 42965-42970.
- <sup>18</sup> L. Chen, L. Wang, Z. Zeng, J. Zhang, Effect of surfactant on the electrodeposition and wear resistance of Ni-Al<sub>2</sub>O<sub>3</sub> composite coatings, *Materials Science and Engineering: A* 434 (2006) 319-325.
- <sup>19</sup> K.H. Hou, M.D. Ger, L. M. Wang, S.T. Ke, The wear behaviour of electro-codeposited Ni-SiC composites, *Wear*, 253 (2002) 994-1003.
- <sup>20</sup> R. L. Zeller, U. Landau, Electrodeposition of Ni-P amorphous alloys, *Journal of the Electrochemical Society* 139 (1992) 3464-3469.
- <sup>21</sup> X.W. Zhou, Y.F. Shen, H.M. Jin, Y.Y. Zheng, Microstructure and depositional mechanism of Ni-P coatings with nano-ceria particles by pulse electrodeposition, *Transactions of Nonferrous Metals Society of China* 22 (2012) 1981-1988.
- <sup>22</sup> Y. He, S.C. Wang, F.C. Walsh, Y.L. Chiu, P.A. Reed, Self-lubricating Ni-P-MoS<sub>2</sub> composite coatings, *Surface & Coatings Technology* 307 (2016) 926-934.
- <sup>23</sup> H.E. Jeong, M.K. Kwak, C.I. Park, K.Y. Suh, Wettability of nanoengineered dual-roughness surfaces fabricated by UV-assisted capillary force lithography, *Journal of Colloid and Interface Science* 339 (2009) 202-207.
- <sup>24</sup> N.D. Boscher, V. Vaché, P. Carminati, P. Grysan, P. Choquet, A simple and scalable approach towards the preparation of superhydrophobic surfaces-importance of the surface roughness skewness, *Journal of material chemistry A* 2 (2014) 5744-5750.

- 
- <sup>25</sup> R.N. Wenzel, Resistance of solid surfaces to wetting by water, *Industrial & Engineering Chemistry* 28 (1936) 988-994.
- <sup>26</sup> A.B.D. Cassie, S. Baxter, Wettability of porous surfaces, *Transaction of Faraday Society* 40 (1944) 546-551.
- <sup>27</sup> F.F. Zhang, B.W. Robinson, H.D. Villiers-Lovelock, R.J.K. Wood, S.C. Wang, Wettability of hierarchically-textured ceramic coatings produced by suspension HVOF spraying, *Journal of Materials Chemistry A* 3 (2015) 13864-13873.
- <sup>28</sup> Q. Yu, Z. Zeng, W. Zhao, Y. Ma, X. Wu, Q. Xue, Patterned Ni-P alloy films prepared by "Reducing-discharging" process and the hydrophobic property, *ACS Applied Materials & Interfaces*, 6 (2014) 1053-1060.